Hindawi
Advances in Materials Science and Engineering
Volume 2024, Article ID 9810320, 1 page
https://doi.org/10.1155/2024/9810320

Retraction

Retracted: Improvement of Microstructure and Properties of Q235 Steel by Iron-Based Laser Cladding Coating

Advances in Materials Science and Engineering

Received 8 January 2024; Accepted 8 January 2024; Published 9 January 2024

This article has been retracted by Hindawi following an investigation undertaken by the publisher [1]. This investigation has uncovered evidence of one or more of the following indicators of systematic manipulation of the publication process:

(1) Discrepancies in scope

(2) Discrepancies in the description of the research reported

(3) Discrepancies between the availability of data and the research described

(4) Inappropriate citations

(5) Incoherent, meaningless and/or irrelevant content included in the article

(6) Manipulated or compromised peer review

The presence of these indicators undermines our confidence in the integrity of the article's content and we cannot, therefore, vouch for its reliability. Please note that this notice is intended solely to alert readers that the content of this article is unreliable. We have not investigated whether authors were aware of or involved in the systematic manipulation of the publication process.

Wiley and Hindawi regrets that the usual quality checks did not identify these issues before publication and have since put additional measures in place to safeguard research integrity.

We wish to credit our own Research Integrity and Research Publishing teams and anonymous and named external researchers and research integrity experts for contributing to this investigation.

The corresponding author, as the representative of all authors, has been given the opportunity to register their agreement or disagreement to this retraction. We have kept a record of any response received.

References

[1] Y. He, Y. Gu, L. Tang, and H. Wang, "Improvement of Microstructure and Properties of Q235 Steel by Iron-Based Laser Cladding Coating," *Advances in Materials Science and Engineering*, vol. 2022, Article ID 2790770, 9 pages, 2022.

Hindawi
Advances in Materials Science and Engineering
Volume 2022, Article ID 2790770, 9 pages
https://doi.org/10.1155/2022/2790770

Research Article

Improvement of Microstructure and Properties of Q235 Steel by Iron-Based Laser Cladding Coating

Yuanwei He,[1] Yu Gu,[1] Li Tang,[2] and Hu Wang [1]

[1]*Mechanical-Electrical Engineering Faculty, Hunan Institute of Traffic Engineering, Hengyang 421001, China*
[2]*National University of Defense Technology, Changsha 410000, China*

Correspondence should be addressed to Hu Wang; 161849039@masu.edu.cn

Received 18 April 2022; Accepted 13 July 2022; Published 13 August 2022

Academic Editor: Ravi Samikannu

Laser cladding is a repair and surface-strengthening technology for the protection of metal parts. It is an effective method for improving the properties of various metal substrates. The process involves melting and solidifying alloy powder on the surface of the substrate. The aim of the present study was to explore the effect of iron-based alloy laser cladding coating on Q235 substrate. Three types of specimens were obtained from Q235 base material using a 5 kW cross-flow CO_2 laser beam. Sample 1 and sample 2 were obtained by the addition of rosin to the iron-based alloy powder. Sample 3 was obtained through the addition of rosin and vanadium to the iron-based alloy powder. A gas curtain was used to wrap the molten pool of samples 2 and 3. The surface hardness of the specimens was determined using a Rockwell hardness tester, and the tensile strength was evaluated using the universal mechanical testing machine. The microstructure of the cladding coating was explored using an Olympus optical microscope and SEM. The results showed that the average hardness of sample 2 and sample 3 was 6.42% and 19.84% higher than that of sample 1. The average tensile strength of samples 2 and 3 was 7.42% and 10.37% higher than that of sample 1. The grain of sample 3 was finer than that of sample 2, and that of sample 2 was finer than that of sample 1 under the same magnification. Rosin minimized oxidation of the substrate, whereas the gas curtain prevented the entry of air into the molten pool, hence the improved properties of samples 2 and 3 compared with that of sample 1. Rosin and the gas curtain protected the powder from oxidation loss and improved the quality of the cladding coating. The results of the present study show that rosin reduced the oxidation of iron-based powder, whereas vanadium improved the hardness and strength of the substrate as well as refined the grain size.

1. Introduction

Laser forming technology can significantly improve the surface physical, chemical, and mechanical properties of steel parts. This technique is widely used in aviation, automobile, shipbuilding, biomedicine, and other fields. It is a green manufacturing technology extensively used globally [1]. Several factors affect the quality and properties of laser-formed samples. The material used to form the laser layer is the main factor that affects the quality and property of samples. Several studies have been conducted on laser-modified samples using iron-based, nickel-based, and cobalt-based alloy powder materials. Iron-based alloy powder is widely used in the laser forming process owing to its low price and ease of manipulation. However, iron-based alloy powder can be easily oxidized and burned during the laser forming process, resulting in defects such as pores and slag inclusion, which affects the mechanical properties of the final samples [2]. Currently, scholars use protective gas under an atmospheric environment to minimize oxidation of the sample. Air is drawn into the protective gas due to the jet entrainment effect, therefore, oxidation and burning loss occur when using this approach. The use of powder with antioxidation burning loss ability on the laser melting pool significantly improves the properties of the laser-formed sample. In the present study, the transient reducing protective atmosphere formed by gasification and combustion of rosin in the laser molten pool was used to reduce the oxidation and burning loss of alloy powder by oxygen in the atmosphere. In addition, it minimizes defects such as pores and slag inclusion on the sample so as to improve the quality of the final samples [3].

The materials used for the laser cladding process include alloy powder, wire, paste, and rod. Most commonly used materials include iron-based, nickel-based, cobalt-based, ceramic powder, composite powder, and amorphous alloy powder with different particle sizes. Self-fusible alloy powder is an alloy powder with various alloying elements (such as Si and B.) added to Ni, Fe, CO, and other matrix alloys [4–8]. This type of powder has a low melting point and is effective for the cladding process. The ceramic powder has a high melting point and hardness and can be classified as carbide ceramic powder, oxide ceramic powder, and silicide ceramic powder. Composite powder mainly refers to alloy powder formed by combining carbide, oxide, boride, silicide, and other high melting points hard ceramic materials with metal materials. The amorphous shape and low interface energy of amorphous alloy powder provide good wettability properties to the matrix material. Moreover, it melts uniformly during cladding [9–13]. The cladding product has higher yield strength, large elastic strain limit, high wear resistance, and excellent corrosion resistance. The most widely used material during laser cladding remanufacturing is iron-based alloy powder. Iron-based alloy powder has low cost, reliable performance, and wear and corrosion resistance, and meets the needs of laser cladding remanufacturing of key metal parts in mining machinery, engineering machinery, steel, and other industries [14–18].

Laser cladding is an effective method for preparing large-area coatings. It is widely used in improving the surface properties of metal parts and repairing surface damage of mechanical products [19–21]. Laser cladding is a new surface modification and damage repair technology widely used in the fields of coating, repair, and prototype manufacturing. Farahmand and Kovacevic used induction heating composite laser cladding technology to reduce the sensitivity of laser cladding to cracks and pores. The findings showed that the use of induction heating significantly improved the transfer efficiency of tungsten carbide (TC). Bidron et al. conducted a study to eliminate thermal cracks in laser cladding through induction preheating. Preheating by induction heating effectively prevents thermal cracks during laser cladding when the preheating temperature range is 800~1100°C [22–24].

Laser cladding technology is used for the formation of cladding coating with excellent properties such as corrosion resistance, high temperature resistance, wear resistance as well as fatigue resistance on low-performance and low-cost steel to meet various harsh requirements [21, 25–29]. Moreover, it reduces cost, minimizes overuse of scarce and precious materials, reduces energy consumption, reduces pollution, and improves the service life of metal parts. Nickel-based powders are currently the most widely used type, but the cost of these powders is about three times higher than that of iron-based powders [30]. However, the iron-based powder is easily oxidized and burnt during the cladding process. In addition, the prepared cladding coating exhibits several defects such as slag inclusion, pores, and cracks [31]. This limitation can be circumvented by using rosin to coat the surface of the iron alloy powder particles, under the action of the laser beam. Rosin forms a reducing protective atmosphere to protect the molten pool from oxidation. Furthermore, it reduces or even eliminates various defects on the cladding coating, thereby markedly improving the mechanical properties of the cladding coating [32]. Vanadium is used to refine steel structures and grains. Therefore, vanadium is added to the alloy powder, forming stable compounds with carbon and oxygen under the action of high-temperature laser. It is mainly dispersed in the cladding coating in the form of vanadium-carbon (VC) which further improves the mechanical properties of the metal part [33].

2. Experimental Materials and Procedures

2.1. Preparation of the Material and Morphological Analysis. The Q235 steel plate has low cost as well as high compatibility with the wire cutting treatment subjected to the substrate and laser clad coating after the test. Therefore, a Q235 steel plate was selected as the substrate in the present study. A high temperature is used in the process of laser rapid prototyping, leading to bending deformation of the substrate, which affects the formation of the sample. The substrate should be appropriately thick to circumvent the effect of high temperatures. A steel plate with more than 15 mm thickness is suitable for experimental requirements. The bending degree of the whole substrate is not significantly different after the laser experiment when using an appropriate thickness; thus, it has little effect on the experimental results. Both sides of the substrate are crushed with a grinder before the experiment. The substrate is first washed with water and detergent to remove oil and impurities. Subsequently, it is cleaned with clean water, then with ethanol to further remove impurities. The substrate is wiped with acetone after cleaning and then dried with a blower. Furthermore, the substrate is dried in a drying oven. The surface of the steel plate is then sandblasted using a sand blasting machine. Sandblasting removes the remaining oil stains and rust, as well as makes the surface of the substrate rough and reduces reflection of the substrate to the laser, for use in the subsequent experiment.

Rosin was added in excess to the iron-based powder and remained in excess after several experiments and attempts. Slag inclusion occurs when the combustion is not complete, and the hydrogen element in the rosin dissolves the metal, resulting in deterioration of the substrate properties. Formation of the gas is ineffective if an insufficient amount of rosin is used; therefore, it does not play the role of protection from reduction. Several experiments and findings from previous studies indicate that the rosin film coating on the surface of iron-based powder particles exhibited a good effect at the micron level. The iron-based powder particles combined with rosin were observed under a scanning electron microscope, and the findings indicated that rosin uniformly covered the powder particles (Figure 1).

Furthermore, a 5 kW cross-flow CO_2 laser was used for the laser rapid prototyping test. The dried powder was placed on the powder feeding device. The 15 mm Q235 steel plate was placed on the experimental workbench, and the distance between the laser nozzle and the substrate was adjusted. The lateral synchronous powder feeding method was used to scan the substrate along the X direction, with the substrate driven by the NC workbench. The laser parameters obtained

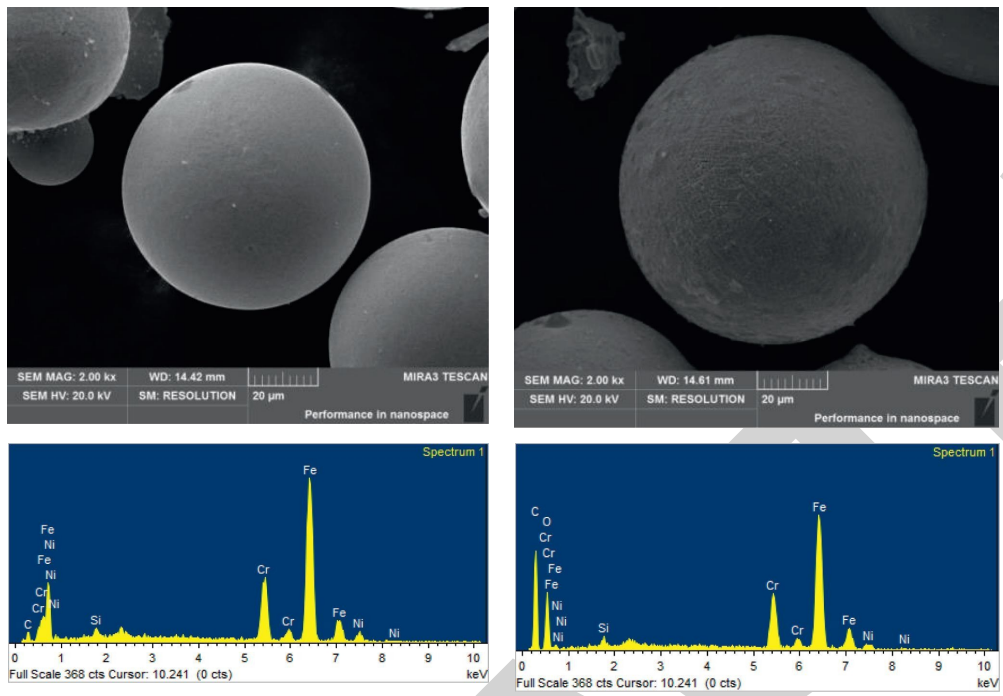

(a) (b)

Figure 1: SEM image of iron-based alloy powder particles: (a) no rosin added and (b) rosin added.

after several experiments are presented in Table 1. The number of scanning layers was 6. The final forming size was approximately 90 mm × 30 mm × 3 mm. The surface of the formed sample did not exhibit any cracks or defects.

The mass percentage of chemical composition of the iron-based alloy powder was C ≦ 0.2%; B ≦ 1.5%; Si ≦ 1.5% Cr = (18~20)%; Ni = (8.0~11)%; and Fe formed the remaining component (Table 1).

The particle size was −150~325 mesh. The mass percentages of chemical compositions of the three powders are shown in Table 2.

Rosin was dissolved in alcohol, and then powders no. 2 and no. 3 were poured into the solvent. The mixture was stirred evenly, dried, crushed, and passed through an 80-mesh sieve. FeCNiBSi was added to the powder to form rosin-coated iron-based alloy powders (FeCNiBSi and FeCNiBSiV). Rosin-coated FeCNiBSi and FeCNiBSiV powders were placed in a drying oven and dried at 45–60°C for more than 8 hours to remove the water in the powder before conducting the experiment. The synchronous powder feeding method was used for drying the powders. The process parameters are presented in Table 3. Model TJ-5050H laser (Wuhan Unity) with 6 scanning layers was used for the experiment. The forming test specimens corresponding to FeCNiBSi powder, rosin-coated FeCNiBSi powder, and rosin-coated FeCNiBSiV powder were labeled as test specimen 1, test specimen 2, and test specimen 3, respectively. The cladding coating was cut through electrode-wire cutting to obtain the nonstandard tensile test specimen as shown in Figure 2.

The iron-based alloy powder without rosin reacts violently with oxygen in the air due to the high temperature of the laser, and the combustion phenomenon was observed (Figure 3). However, the combustion phenomenon was significantly weakened after the addition of rosin. A synchronous powder feeding nozzle device with an outer ring

Table 1: Levels of different elements in the ion-based alloy powder particles (a) before and (b) after addition of rosin.

Element	Weight%	Atomic%
A		
C	10.53	34.87
Si	1.16	1.65
Cr	17.48	13.37
Fe	62.05	44.18
Ni	8.77	5.94
Total	100.00	
B		
C	36.63	63.71
O	13.10	17.11
Si	0.42	0.31
Cr	9.51	3.82
Fe	38.37	14.35
Ni	1.97	0.70
Totals	100.00	

Table 2: Composition of the three types of powders.

No.	Composition		
	Iron-based alloy powder (%)	Rosins (rosin)	*V*
1	100	—	—
2	99.4	0.6%	—
3	99.2	0.6%	0.2%

Table 3: Laser process parameters.

Power	Scanning speed	Spot size	Synchronous powder feeding speed	Protective gas	Overlap rate (%)
2.2kw	6 mm/min	3 ∗ 5 mm	6 g/min	Argon	50

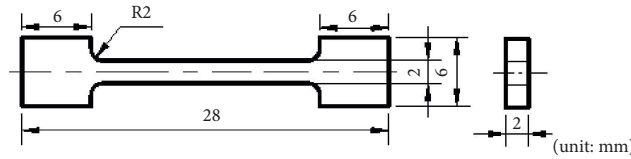

Figure 2: Schematic diagram of tensile test specimen.

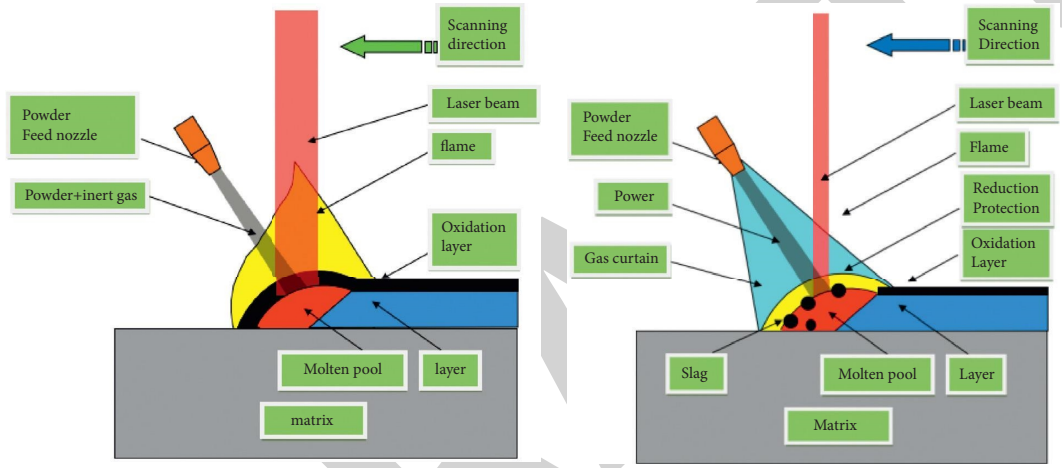

Figure 3: Schematic diagram showing the laser cladding process. (a) Formation of the laser cladding coating without the addition of rosin. (b) Formation of the laser cladding coating after addition of rosin under outer ring protective gas curtain.

protective gas curtain was used to further reduce the oxidation and burning loss of iron-based alloy powder during the cladding process. Argon gas was used in the cladding process. The reduction protection zone formed by rosin firstly reacted with oxygen to protect the molten pool, and the nozzle released the outer ring protective gas curtain to cover the reduction protection zone formed by rosin to further prevent reaction with oxygen and strengthen the protection of the molten pool.

The formation of the laser layer cladding without the gas curtain and after the application of a gas curtain is presented in Figure 4. The results showed that the oxidation phenomenon was more evident without the gas curtain (Figure 4(a)) than with the presence of the gas curtain (Figure 4(b)).

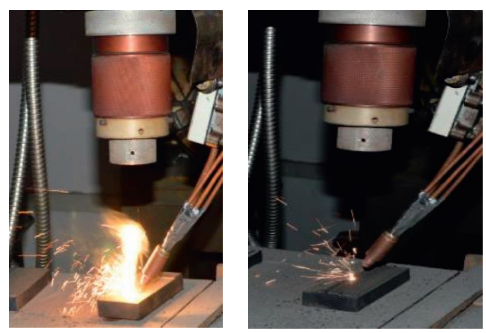

(a) (b)

Figure 4: Oxidation of the sample during the cladding process (a) without a gas curtain and (b) with a gas curtain.

2.1.1. Hardness Test. The sample surface was cleaned with acetone to remove foreign matters introduced after grinding the surface of the cladding coating. The TH320 Rockwell hardness tester was then used to determine the hardness of 10 randomly selected points on the surface of the sample. The average value of microhardness was determined after eliminating minimum and maximum values. The microhardness of the three samples was determined every 0.2 mm along the depth direction from the coating to the substrate. A 6 s holding time was used with a test load of 150 kg (1471 N) to determine the sample hardness.

2.1.2. Microstructure Analysis. A small part (10 mm × 10 mm × 15 mm) of each of the three test specimens was obtained by wire-electrode cutting. The test specimens were polished using coarse- to fine-grade sandpaper to obtain

metallographic specimens. Subsequently, the specimens were treated with aqua regia, and then observed under an OLYMPUS GX51F optical microscope. Furthermore, the microstructures of the test samples were observed using a TESCAN MIRA3 LMU JSM-6701F scanning electron microscope. The phase components of the samples were determined by X-ray diffraction (XRD-7000 S Shimadzu, Japan). The X-ray source for the process was Cu-Kα radiation at 40 kV and 200 mA. The samples were scanned at an angular 2 θ angle between 20° and 80° with a step size of 0.2° and a collection time of 10 s.

2.1.3. Tensile Property Test. An electrohydraulic servo dynamic and static universal testing machine PWS-E100 (Jinan) was used to test the tensile properties of the specimen. The specimens were polished using sandpaper to remove the wire-cut marks on the surface before conducting the tensile test. Subsequently, the samples were then mounted on the self-made fixture. Experiments were carried out at room temperature with a tensile rate of 0.2 mm/min.

3. Analysis of the Experimental Results

3.1. Appearance and Morphology of the Specimen. The morphology of the cladding coating was observed after the cladding coating was formed. The findings showed that the laser cladding coating without rosin was covered with an oxide film and had no metallic luster, whereas the laser cladding coating with rosin had evident metallic luster (Figure 5). The experimental results showed that the addition of rosin effectively reduced the oxidation and burning loss of iron-based alloy powder. Notably, oxidation was further reduced under the protection of a gas curtain.

Morphology analysis of the laser-forming sample showed the highest level of oxidation for the sample without rosin and gas curtain, moderate level of oxidation for the sample with rosin but without the gas curtain, and the least oxidation for the sample with rosin and the gas curtain (Figure 5).

3.2. Hardness Analysis. The values of the hardness of each specimen are shown in Figure 6. The average Rockwell hardness values of test specimen 1, test specimen 2, and test specimen 3 were 26.96 HRC, 28.69 HRC, and 32.31 HRC, respectively (Figure 6). The results showed that the hardness level of test specimen 2 was 6.41% higher compared than that of test specimen 1. The hardness level of test specimen 3 was 12.62% higher than that of test specimen 2. The findings indicated that the hardness of the cladding coating was improved by adding rosin and vanadium. The hardness of vanadium-carbon produced by combining vanadium and carbon at high temperature was high because it was dispersed in the cladding coating, hence increasing the hardness of the sample.

3.3. Tensile Property Analysis. Furthermore, the tensile strength of the three specimens was determined (Table 4). The findings showed that the average tensile strength of test specimen 3 was 2.7% higher than that of test specimen 2, and 10.37% higher than that of test specimen 1. The average tensile strength of test specimen 2 was 7.4% higher than that of test specimen 1. The findings indicate that the addition of rosin and V to the powder improved the average tensile strength of the test specimen, with a more significant effect observed after the addition of rosin. Oxidation and burning loss of the iron-based powder were markedly reduced after the addition of rosin, thereby significantly reducing the defects in the cladding coating. This explains the significant effect on improving the tensile strength of the specimen (see Figure 7).

3.4. Microstructure Analysis. The laser rapid prototyping process comprises sudden heating and rapid cooling. The grains in the formed sample were small and dense because the crystal nucleus had no time to grow during the forming process. The structure showed a growth trend with an increase in temperature. Therefore, the hardness, tensile strength, and fatigue properties of the sample were significantly higher than the properties of the casting. The findings showed that the structure of each sample had a specific characteristic (Figure 8). The specimens presented a dendritic structure. The microstructure of sample 2 after the addition of rosin was finer compared with that of sample 1. Notably, sample 3 showed the finest microstructure. The oxidation and burning loss of various alloy elements in sample 2 and sample 3 were markedly reduced; hence, the effect of alloy grain refinement was significant. Vanadium was added to sample 3 to improve the nucleation rate, and the microstructure was finer. The dispersion strengthening effect of sample 2 and sample 3 alloy elements was higher than that of sample 1. The findings indicate that the addition of rosin to the sample reduced the burning loss of alloy elements and enhanced the grain refining effect of alloy elements. This explains the effect of dispersion strengthening and the effect of solid solution strengthening in sample 2 and sample 3. In addition, the microhardness and increase in tensile strength, and improvement of fatigue properties are attributed to the ability of rosin to reduce the burning loss.

Further microstructure analysis of the test samples was conducted by observing the samples under the TESCAN MIRA3 LMU JSM-6701F scanning electron microscope. The microstructure of test specimen 1 was coarser, the microstructure of test specimen 2 exhibited a fine-grained structure, and the microstructure of test specimen 3 exhibited a high nucleation rate and more evident refinement (Figure 9). This finding indicates that the tensile property of test specimen 3 was better than that of test specimen 2 and test specimen 1. The experimental results showed that the addition of rosin and vanadium refined microstructure grains and optimized the mechanical properties of the cladding coating.

(a) (b) (c)

Figure 5: Macromorphology variation of the laser forming samples. (a) Sample without rosin and a gas curtain. (b) Sample with rosin but without a gas curtain. (c) Sample with rosin and a gas curtain.

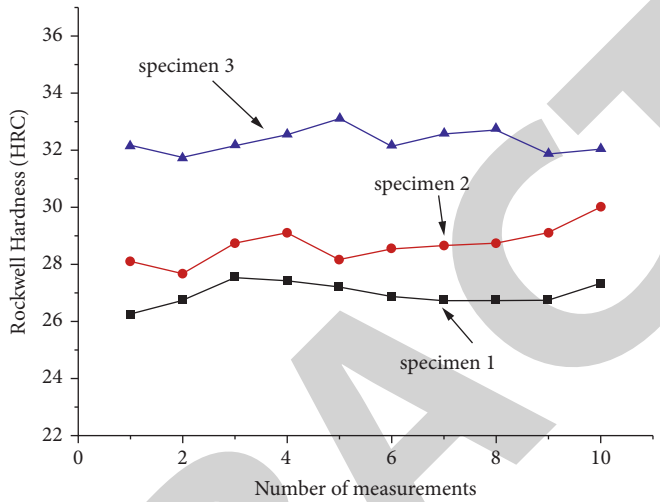

Figure 6: Rockwell hardness of the three test specimens.

Table 4: Tensile strength of the three test specimens.

Test specimen no.	Tensile strength (MPa)			Average (MPa)
Test specimen 1	922	917	909	916
Test specimen 2	998	971	983	984
Test specimen 3	1003	1009	1021	1011

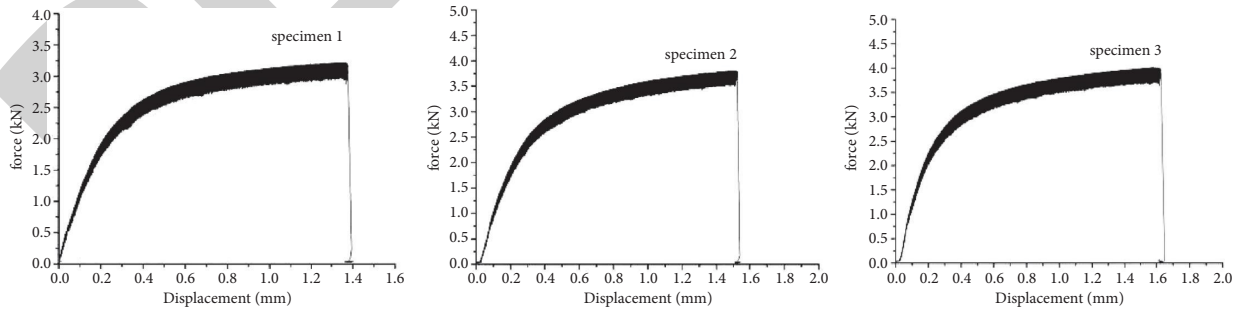

Figure 7: Stress-strain curves of the three specimens: specimen 1 (cross-sectional area: 3.50 mm^2); specimen 2 (cross-sectional area: 3.82 mm^2); specimen 3 (cross-sectional area: 4.00 mm^2).

3.5. XRD Analysis. XRD analysis showed that the cladding coating mainly comprised the α-Fe phase and γ-Fe phase. The spectra of the three samples and the position of the diffraction peak were compared. The findings showed that the intensity of the austenite diffraction peak generated by sample 3 was stronger than that of sample 2, and the intensity of the diffraction peak for sample 2 was stronger than that of sample 1 (Figure 10). This further verifies that the rosin coating on the surface of the alloy powder played a chemical protection role during laser cladding. Rosin

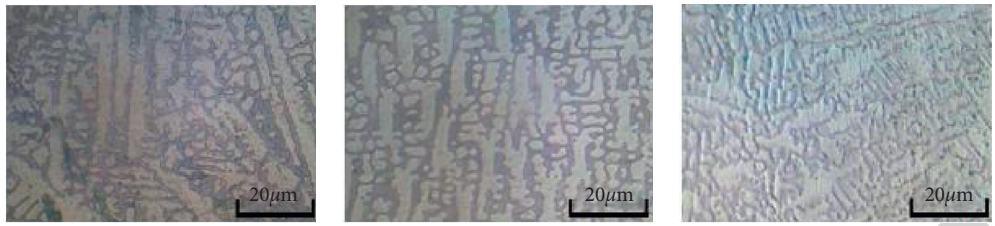

Figure 8: Morphology of the three specimens: (a) microstructure diagram of test specimen 1; (b) microstructure diagram of test specimen 2; (c) microstructure diagram of test specimen 3.

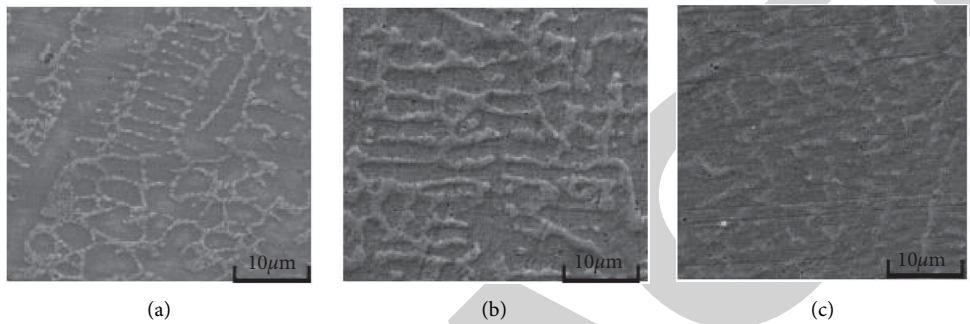

Figure 9: SEM images showing microstructure of the three samples: (a) SEM image of test specimen 1; (b) SEM image of test specimen 2; (c) SEM image of test specimen 3.

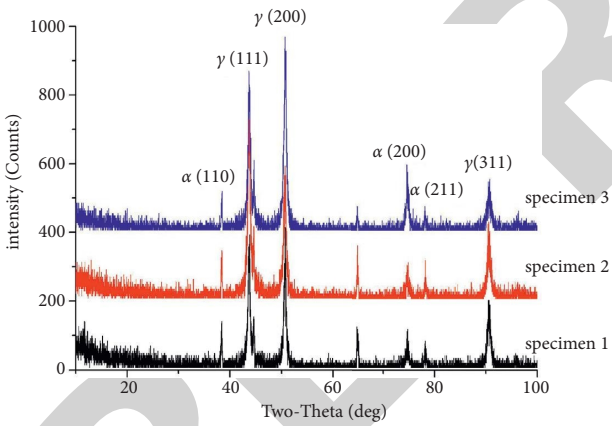

Figure 10: XRD patterns of the three specimens.

weakened the oxidative burning loss of iron-based alloy powder as well as reduced the burning loss of medium elements resulting in a high-intensity peak value.

4. Conclusion

The findings of the present study show that the rosin film coated on the surface of powder particles protects the molten pool during laser cladding. In addition, it prevents oxidation of liquid metal and minimizes oxidation and burning loss of the iron-based alloy powder during cladding. Moreover, rosin coating minimizes defects such as slag inclusion. Furthermore, the rosin refines the microstructure grains, and improves the mechanical properties of the cladding coating. Furthermore, a combination of rosin and gas curtain minimizes the entry of air into the molten powder, which further reduces oxidation.

The addition of rosin to iron-based alloy powder minimizes the loss of alloying elements and increases the effect of alloying elements. This increases the dispersion strengthening phase as well as causes segregation of the alloy element, resulting in increase in the value of Rockwell hardness and tensile strength.

Vanadium and carbon combine to form vanadium-carbon, which has a high level of hardness. This property causes dispersion of the cladding coating and significantly increases the hardness of the sample. Moreover, vanadium increases the nucleation rate and plays a significant role in grain refinement.

Data Availability

The datasets used and analysed during the current study are available from the corresponding author upon reasonable request.

Conflicts of Interest

The authors declare that they have no conflicts of interest.

Acknowledgments

This work was supported by the Natural Science Foundation of Hunan Province (2020JJ6091).

References

[1] J. Li and S. Pogodin, ""Made in China 2025": China experience in industry 4.0," *IOP Conference Series: Materials Science and Engineering*, vol. 497, no. 1, Article ID 012079, 2019.

[2] J. Laeng, J. G. Stewart, and F. W. Liou, "Laser metal forming processes for rapid prototyping -a review," *International Journal of Production Research*, vol. 38, no. 16, 2000.

[3] D. W. Deng, J. H. Sun, and X. L. Wang, "Effect of laser power on the structure and properties of laser cladding nickel-based alloy coating," *Chinese Journal of rare Metals*, vol. 40, no. 1, p. 20, 2016, in Chinese.

[4] A. Gopalakrishnan, M. Rajkumar, J. Sun, and J. P. Trilles, "Occurrence of double parasitism on black-barred halfbeak fish from the southeast coast of India," *Chinese Journal of Oceanology and Limnology*, vol. 28, no. 4, pp. 832–835, 2010.

[5] S. Singh, P. Kumar, D. K. Goyal, and A. Bansal, "Erosion behavior of laser cladded Colmonoy-6 + 50%WC on SS410 steel under accelerated slurry erosion testing," *International Journal of Refractory Metals and Hard Materials*, vol. 98, Article ID 105573, 2021.

[6] S. Roy, N. Sridharan, E. Cakmak, H. Ghaednia, A. Gangopadhyay, and J. Qu, "Post weld heat treatment and operating temperature effect on tribological behavior of laser cladded stellite 21 coating," *Wear*, vol. 482–483, Article ID 203990, 2021.

[7] F. A. d. Lucena, G. Y. Koga, R. Riva, and C. R. M. Afonso, "Production and characterization of laser cladding coating of Fe66Co7Nb4B23 (at.%) gas-atomized and ball-milled powders," *Journal of Materials Research and Technology*, vol. 14, pp. 2267–2280, 2021.

[8] S. T. Nyadongo, E. O. Olakanmi, and S. L. Pityana, "Experimental and numerical analyses of geometrical and microstructural features of Tribaloy T-800 composite coating deposited via laser cladding-assisted with pre-heat (LCAP) process," *Journal of Manufacturing Processes*, vol. 69, pp. 84–111, 2021.

[9] S. Bajda, Y. Liu, R. Tosi et al., "Laser cladding of bioactive glass coating on pure titanium substrate with highly refined grain structure," *Journal of the Mechanical Behavior of Biomedical Materials*, vol. 119, Article ID 104519, 2021.

[10] A. Malachowska, G. Paczkowski, T. Lampke, and A. Ambroziak, "Characterization of FeP-based metallic glass coatings prepared with laser cladding," *Surface and Coatings Technology*, vol. 405, Article ID 126733, 2021.

[11] N. N. Soboleva and A. V. Makarov, "Effect of conditions of high-temperature treatment on the structure and tribological properties of nickel-based laser-clad coating," *Russian Journal of Non-ferrous Metals*, vol. 62, no. 6, pp. 682–691, 2022.

[12] L. Shen and T. Yamaguchi, "High-temperature oxidation behavior of laser-cladded refractory NiSi0.5CrCoMoNb0.75 high-entropy coating," *Journal of Materials Research and Technology*, vol. 17, 2022.

[13] Q. Wang, R. Qian, J. Yang et al., "Effect of high-speed powder feeding on microstructure and tribological properties of Fe-based coatings by laser cladding," *Coatings*, vol. 11, no. 12, 2021.

[14] H. Ge, H. Fang, C. Zhang, L. Wang, Q. Zhang, and J. Yao, "The evolution of element distribution during laser cladding under static magnetic field," *Metallurgical and Materials Transactions A*, prepublish, 2021.

[15] T. Perrin, A. Sofiane, M. Pierre-Jean, and S. Frederic, "Characterization of WC-doped NiCrBSi coatings deposited by Laser Cladding; effects of particle size and content of WC powder," *Surface and Coatings Technology*, vol. 425, 2021.

[16] Y. Zhao, Y. Chen, T. Zhang, and T. Yu, "Laser fabricated nickel-based coating with different overlap modes," *Materials and Manufacturing Processes*, vol. 36, no. 14, pp. 1618–1630, 2021.

[17] M. Zeng, H. Yan, B. Yu, and Z. Hu, "Microstructure, microhardness and corrosion resistance of laser cladding Ni–WC coating on AlSi5Cu1Mg alloy," *Transactions of Nonferrous Metals Society of China*, vol. 31, no. 9, pp. 2716–2728, 2021.

[18] D. Zhang, Z. Li, H. Fan, H. Rui, and F. Gao, "Microstructure and tribological properties of Fe-based laser cladding layer on nodular cast iron for surface remanufacturing," *Coatings*, vol. 11, no. 8, 2021.

[19] S. Nam, H. W. Lee, I. Jung, and Y. M. Kim, "Microstructural characterization of TiC-reinforced metal matrix composites fabricated by laser cladding using FeCrCoNiAlTiC high entropy alloy powder," *Applied Sciences*, vol. 11, no. 14, 2021.

[20] J. Dong, H. Gao, and J. Shen, "Development and application of laser remanufacturing technology," *Mining Machinery*, vol. 47, no. 1, pp. 1–6, 2019.

[21] J. Liu, M. Song, C. Chen, and H. Yu, "Research progress of laser cladding technology on titanium alloy surface," *Metal Heat Treatment*, vol. 44, no. 5, pp. 87–96, 2019.

[22] Q. Ai, X. Feng, J. Cao, and Z. Su, "Research progress of laser cladding technologyly," *Materials Review: Review*, pp. 24–32, 2010.

[23] T. Yu, B. Song, W. Xi, and Y. Zhao, "Analysis on effect of process parameters on laser cladding of iron-based alloy powder," *Hot Working Technology*, vol. 1-5, 2021.

[24] S. Zhao, Y. Guo, R. Chai, and M. Yao, "Effect of scanning speed on the microstructure and properties of laser-clad iron-based alloys," *Applied Laser*, vol. 40, no. 5, pp. 811–820, 2020.

[25] B. Yang, Z. Wang, J. Zuo, X. Jiang, and X. Zhang, "Iron-based composite coating prepared by laser cladding and its heat and corrosion resistance," *Chinese Journal of Lasers*, vol. 47, no. 10, pp. 38–44, 2020.

[26] G. Wei, Z. Liping, X. Chao, and C. Rongxia, "Findings from xi'an university of science and technology in the area of materials research described (study on the wear resistance of laser cladding iron-base alloy by heat treatment)," *Journal of Technology*, vol. 6, 2019.

[27] P. Farahmand and R. Kovacevic, "Laser cladding assisted with an induction heater (LCAIH) of Ni – 60% WC coating," *Journal of Materials Processing Technology*, vol. 222, pp. 244–258, 2015.

[28] G. Bidron, A. Doghri, T. Malot, M. Thomas, and P. Peyre, "Reduction of the hot cracking sensitivity of CM - 247LC superalloy processed by laser cladding using induction preheating," *Journal of Materials Processing Technology*, vol. 277, Article ID 116461, 2019.

[29] V. Kotlan, R. Hamar, P. David, and D. Ivo, "Model of depositing layer on cylindrical surface produced by induction-assisted laser cladding process," *Open Physics*, vol. 15, no. 1, pp. 971–978, 2017.

[30] H. Zhang, Z. Sun, F. Li, H. Chang, and F. Xing, "Effect of microstructure and properties of iron-based composite coating prepared by laser cladding," *Surface Technology*, vol. 47, no. 12, pp. 127–133, 2018.

[31] H. Zhu, Y. Li, Z. Zhang, B. He, and C. Qiu, "Mechanical and corrosion properties of martensite/ferrite duplex stainless steel prepared via laser cladding," *Chinese Journal of Lasers*, vol. 45, no. 12, pp. 148–153, 2018.

[32] Y. Cai, L. Zhu, Y. Cui, and K. Geng, "Influence of high-temperature condition on the microstructure and properties of FeCoCrNiAl;and FeCoCrNiAl;high-entropy alloy coatings," *Surface Engineering*, vol. 37, no. 2, 2021.

[33] P. Yang, Y. Song, J. Wang, F. Hu, and L. Xie, "Semiconductor laser cladding of an iron-based alloy on nodular cast iron," *Welding in the World*, (prepublish), 2021.